Chapter 3
The Use of Micro–computed Tomography for Forensic Applications

Sarah V. Hainsworth

Introduction

Wilhelm Röntgen discovered the electromagnetic radiation known as X–rays in 1895. One of Röntgens first images was of his wife's hand which showed the structure of the hand and bones beneath the skin. X–rays travel from the X–ray source through the object (patient) being examined and are captured on an X–ray detector, originally a photographic plate but now using an electronic detector, to create an image known as a radiograph which gives a 2D representation of the object [1].

X–rays are absorbed in different amounts depending on the radiological density represented by the Hounsfield number, symbol HU [2] of the material being examined. Different materials therefore give different contrasts in the final image, depending on their radiological density. The radiological density is a function of the density of the material and the atomic number. The HU values are measured based on zero HU being defined as the radiodensity of distilled water at standard temperature (STP) and –1000HU being the radiodensity of air at STP. The HU value is calculated from

$$\mathrm{HU} = 1000 \times (\mu - \mu_{\mathrm{water}}/\mu_{\mathrm{water}} - \mu_{\mathrm{air}})$$

where μ = linear attenuation coefficient of substance, μ_{water} = linear attenuation coefficient of water, and μ_{air} = linear attenuation of air. Bone, which contains calcium for example, has a higher atomic number than most tissues and therefore bones absorb X–rays more readily to give a higher contrast than tissues and bony structures. This is why they appear white against a black background in a radiograph (HU cortical bone ~ +1000 or very dense bone +2000). Tissues like fat and muscle or air–cavities like the lungs give a darker grey shade on the radiograph [2]. Metals typically have

S. V. Hainsworth (✉)

University of Bath, Claverton Down, Bath, UK

e-mail: sh2933@bath.ac.uk

a HU of 3000 [3]. The ability of X–rays to discriminate between fat, tissue, muscle, bone and fractures have thus meant that they have been commonly used as a medical diagnostic tool since their discovery.

The first forensic use of X–rays followed very quickly after their discovery as it was realised that foreign objects such as needles and bullets could easily be located on an X–ray radiograph [1]. Professor Arthur Schuster, a physicist at Owens College in Manchester, England used X–rays in the case of a gunshot wound to locate a bullet fired by Hargreaves Hartley, into the brain of his wife Elizabeth Ann Hartley at Nelson, Lancashire, on 23 April 1896 [4, 5]. The bullets were located but Elizabeth Hartley died shortly afterwards from her injuries.

In the early 1950s, Godfrey Hounsfield from EMI in the UK and Allan Cormack from Tufts University in the USA were separately and simultaneously instrumental in working out that the internal structure of an object could be determined from multiple X–ray images taken at various angles. They were subsequently awarded the Nobel Prize for Physiology or Medicine in 1979 [6] for the development of X–ray computed tomography. Their work showed that 3D representations of objects could be achieved by taking multiple 2D radiographs and computationally reconstructing 3D tomograms of the internal structure of the object that can be used for visualisation and quantification. The advent of storing radiographs digitally by capturing the X–rays on flat screen detectors has meant that access to computing tools to reconstruct the images in 3D becomes much more accessible than was the case with wet chemical photographic plates and along with modern computing capabilities has vastly transformed the way in which images can be recorded and manipulated to gain insights into 3D structures.

Conventional multi–detector computed tomography (MDCT) is widely used in medicine [7, 8] and has been adopted, along with MRI, as an essential tool in forensic applications for many of years [9, 10]. Computed tomography uses X–ray projections taken at multiple angles of view about an axis through an object to make a 3D reconstruction using an algorithm [11]. It is widely used in post mortem imaging and has become recognised as having the capability of allowing virtual autopsies [12], although not all forensic practices have ready access to the scanners.

One of the disadvantages of multi–detector computed tomography (MDCT) is that it has a relatively low resolution and a fixed magnification. For higher resolution X–ray imaging, Cone Beam Computed Tomography (CBCT) can image smaller areas with higher magnifications [13, 14]. This technique is commonly used for dental X–rays [15] and breast examination [16].

When higher resolution than cone beam tomography is needed then micro– or nano–CT [17] systems, often found in engineering or materials science research, can be used. Micro– and nano–CT are used for studying materials, foods, and samples from biology, geology and palaeontology. The scans can also be used for metrology and accurate characterisation of dimensions of internal structures produced during manufacturing. Nano–CT is outside the scope of this chapter as it commonly requires high–resolution X–rays from a synchrotron storage ring. Micro computed tomography (μCT) was developed in the early 1980s [17, 18]. The term applies to X–ray tomography with voxel (volume element) resolutions that are typically between 1

and 50 µm. Mini–CT typically has voxel resolutions between 50 and 200 µm and nano–CT has voxel resolutions between 0.1 and 1 µm. However, micro–, mini– and nano–CT are all often described generically as µCT. µCT has become an increasingly important technique since its inception because it has a number of advantages including:

- Quick and easy radiographic inspection
- Exceptional resolution
- Photo–realistic reconstruction
- Non–destructive
- Little or no preparation of specimens other than securely mounting
- Intuitive visualisation that brings results to life
- Ability to create 3D replicas using modern 3D printing tools.

µCT is attractive for forensic applications as it can provide images which have much higher magnifications and resolutions than that achievable in clinical CT scanners [19].

Another form of CT is industrial computed tomography [20–22] that was also developed from medical CT. It is widely used for industrial inspection, for quality control of complex three–dimensional engineering components and for inspection of assemblies of parts. There are two types of industrial CT scanners:– some use a cone–shaped X–ray beam and flat–panel type of detector as is used in µCT; whereas others use a collimated fan–shaped beam with a detector in a line–scanning mode. Industrial CT can be used for flaw detection, engineering failure analysis, and metrology (inspection of the dimensions of components and in particular internal features that cannot otherwise be measured using e.g. laser scanning or touch probes). Additionally, industrial metrology can be used for reverse engineering of components. Industrial scanning has potential forensic uses in engineering, for example, inspections of gear boxes/air bags/switches or other components that might have failed. Other forensic uses can include examination of firearms, or explosive devices, and searching for concealed compartments [23]. Industrial CT can also be used for applications in forensic anthropology when access to MDCT or µCT is not available [23].

Table 3.1 compares the typical size of objects that can be imaged, resolution, and X–ray energy for the different types of tomography. All X–ray CT systems rely on the absorption of X–ray photons. This gives limits to the volume of objects that can be scanned as if all the photons are absorbed before the detector then there are no data. Higher atomic number materials/denser materials absorb X–rays more readily than lower atomic materials/lower density materials and thus the largest volume that can be measured is limited by the volume that allows analysis of the X–rays reaching the detector.

One disadvantage of µCT techniques is that they usually require a further analysis, for example by scanning electron microscopy with energy dispersive X–ray analysis or other chemical analysis by X–ray diffraction, to determine the chemical composition or phase of a foreign material within a sample or specimen. One way in which CT can become more useful in determining the chemistry of the body is by measuring the HU values of common materials found in forensic pathology, including

Table 3.1 A comparison of the different object sizes, resolution and X–ray energy for a number of different 3D X–ray computed tomography modalities

	Object size	Resolution (Voxel size)	X–ray energy
Medical multidetector CT	Whole human body can be imaged Typical engineering component such as an automobile cylinder head which fits through scanning ring	≥100 µm	80–140 keV
Medical cone beam CT	Dental scanners will allow head and jaw to be imaged	500 µm	60–90 keV
Micro CT	Varies but 280 mm diameter by 600 mm height is typical for a cone–beam system where the specimen rotates	≥0.1 µm	30–300 keV
Industrial CT	Varies but typically 0.8 × 1.2 m part envelope	~0.5 µm	>450 keV

steels, brass, aluminium for example, glass, rocks or other man–made materials to produce a reference set of materials that can aid identification [24]. These materials can then be incorporated into phantom samples (a specially designed object with defined components and composition) that can be scanned alongside the sample of interest.

Instrumentation

Figure 3.1 illustrates the two types of arrangements that are commonly used in µCT scanners. In the first, a specimen is scanned by rotating it around a vertical axis whilst the X–ray source and detector are static. In the second (typically used for scanning small animals) the sample is positioned horizontally and the X–ray source and detector are rotated around a horizontal axis through the animal.

The size of sample that can be imaged in a µCT is determined by the space between the source and the detector. A sample must be able to sit on the rotation platform and be rotated in a stable manner without impeding (touching) the detector or source. In order to be able to exactly reconstruct the 3D image, the specimen has to stay in the field of view (FOV) for all rotations.

The time taken for a scan depends on the number of radiographs that are taken and the time for an individual radiograph to be taken. The time for an individual radiograph depends on the X–ray flux that is generated by the X–ray source and the absorption of the X–rays by the sample. The flux determines the time required to
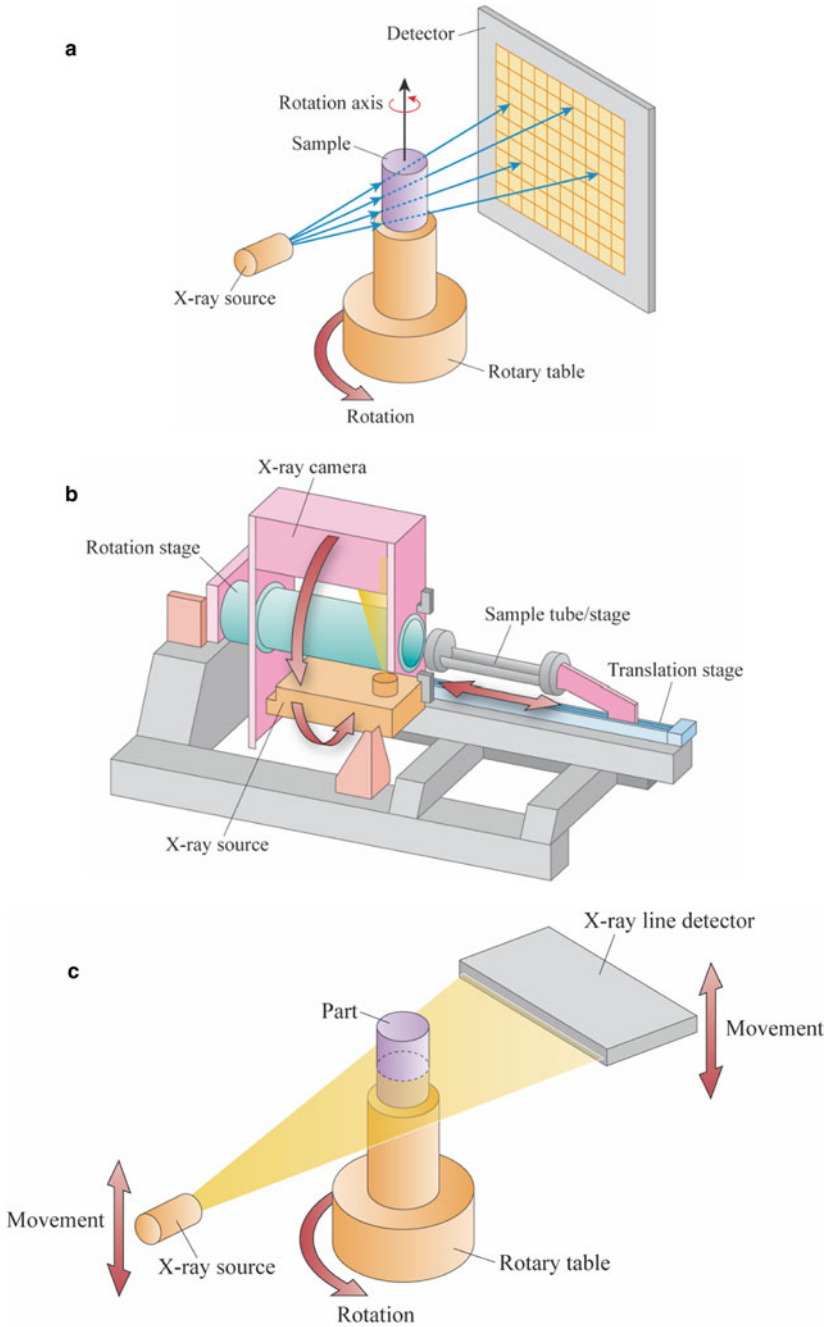
Fig. 3.1 Common X–ray computed tomography configurations **a** cone beam system typical of many laboratory systems **b** small animal μCT scanner configuration **c** set–up for an industrial X–ray CT line scanner. Illustrations courtesy of Vicky Eves, UK

obtain a projection image of the required quality dependent on the signal–to–noise ratio and obtaining a good dynamic range of contrast. The X–ray flux and exposure time will determine the number of X–ray photons incident per image pixel. It is important that the detector is not over–saturated by photons. The contrast sensitivity is determined by the characteristics of the specimen and also the instrument characteristics.

A typical laboratory µCT system with the configuration shown in Fig. 3.1a is shown in Fig. 3.2.

The noise in the reconstructions can be decreased by using frame averaging as long as the incident X–ray beam is stable. Essentially, this consists of acquiring multiple images at each rotation step which are then averaged to get the final image projection that is used for reconstruction with an improved signal–to–noise ratio. Depending on the detector, four frame averages with a 12 bit detector are comparable to a 14 bit detector i.e. in terms of the ability to discriminate between pixels of different grey levels. It is not possible to get a valid reconstruction if the detector saturates at any point in the image.
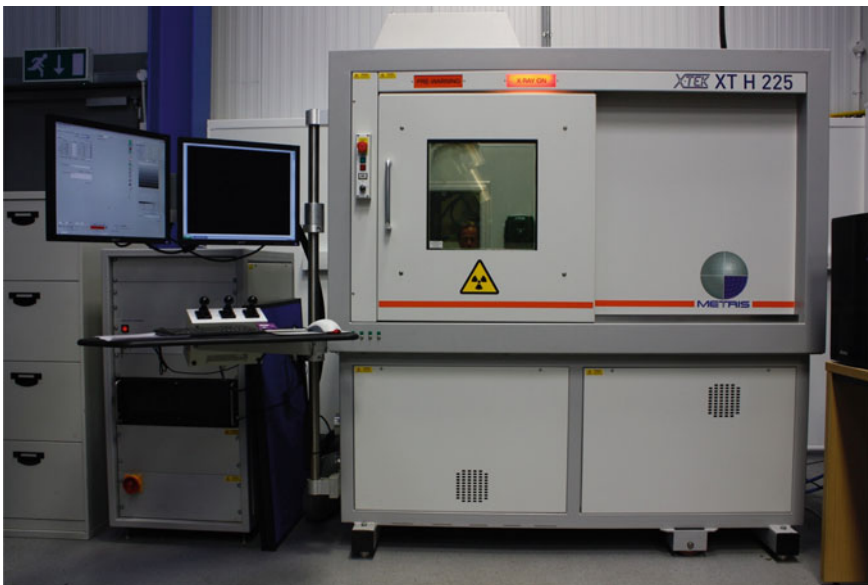

Fig. 3.2 A Nikon XT H225 micro computed tomography scanner in the Department of Engineering at the University of Leicester showing the sample chamber and control monitors for setting up the scans

Magnification, Resolution and Quantification

The magnification M in a µCT system is is defined as the ratio of the focus–to–detector distance over the focus–to–sample distance, i.e. M = FDD/FOD as shown in Fig. 3.3.

The spatial resolution of X–ray CT systems is influenced by a number of factors including the focal spot size, X–ray detector performance, system magnification, number of projections, filtering and the reconstruction algorithms that are used.

The spatial resolution is usually defined by the voxel size which is a function of the pixel size divided by the magnification. The spatial resolution is defined by how far two features of the object need to be separated to be distinguishable in the measured image [25]. This can either be determined by visual resolution tests using line group test patterns (which are observer dependent) where the resolution is defined by when two distinct lines cannot be separated or by using modulation transfer functions [26].

If µCT is being used for metrology purposes to derive quantitative data from the images, then it is important that the spatial resolution and other sources of error in the data are well understood. Additionally, it is important for the validity of measurements and their interpretation that measurements are both reproducible and repeatable i.e. that here is agreement of results from experiments performed in the same way under the same conditions and also for repeated measurements of a single sample under the same conditions. It is important that appropriate calibrations are performed [20, 27]. Additionally, variables during the measurements should be carefully controlled. These can include factors related to the CT systems:– the measurement object itself, the analysis method of the scans, the environment for scanning such as temperature and, humidity, and finally the operator using the same scanning parameters for repeated measurements.
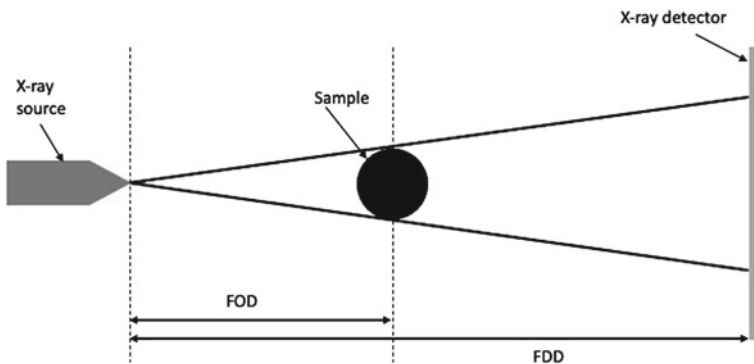

Fig. 3.3 Image magnification for µCT. FOD is the focus to sample distance and FDD is the Focus to detector distance

Software

An important part of any analysis by X–ray CT is image reconstruction. The reconstruction of images is challenging as every voxel has between 8–16 bits of grayscale information and a 3D volume image may have between 500^3 and 2000^3 voxels. This tends to lead to large files and a need for considerable computing power for image storage, transfer and display.

Most X–ray CT manufacturers have their own proprietary software for reconstruction. Most of these use a reconstruction method based on filtered back–projection which is based on an algorithm developed by Feldkamp [28]. In addition, there are a number of commercial software packages such as VGStudio MAX (Volume Graphics, GmbH) Avizo (VSG Visualization Sciences Group, Mérignac, France), and Simpleware (Simpleware Ltd., UK) which is a volumetric data processing software that can export volumetric data into CAD and finite element models. There are also a number of valuable freeware resources including Drishti [29], Image J [30] and Dragonfly (Object Research Systems Inc., Montreal, Canada) although others are also freely available.

Potential Sources of Error

There are several potential sources of error in μCT. These can be physical–based, scanner–based, or sample–based.

In scanners where the source and detector rotate around the sample, it is critical that the source and detector rotate so that deviation from the required ideal trajectory around the axis of rotation is smaller than the detector pixel size. Sample mounting is also important to avoid motion artefacts from the sample moving during scanning or dynamic changes occurring during scanning through for example heating or a hydrated sample drying out. Motion artefacts can also arise during dynamic scanning from the sample itself moving (such as a fly hatching).

Beam Hardening

X–ray beams have photons of different energies. Beam hardening is an artefact that occurs as the X–ray beam passes through an object as the lower energy X–rays are absorbed preferentially and higher energy X–ray photons remain. This means that the beam becomes "harder," i.e. its mean energy increases since lower energy photons are absorbed more rapidly than the higher–energy photons. Beam hardening can lead to uneven contrast from the outside to the inside of the sample. This is known as a cupping artefact (Fig. 3.4). Beam hardening can be reduced by using a physical filter of a material that absorbs the lower energy X–rays placed between the X–ray

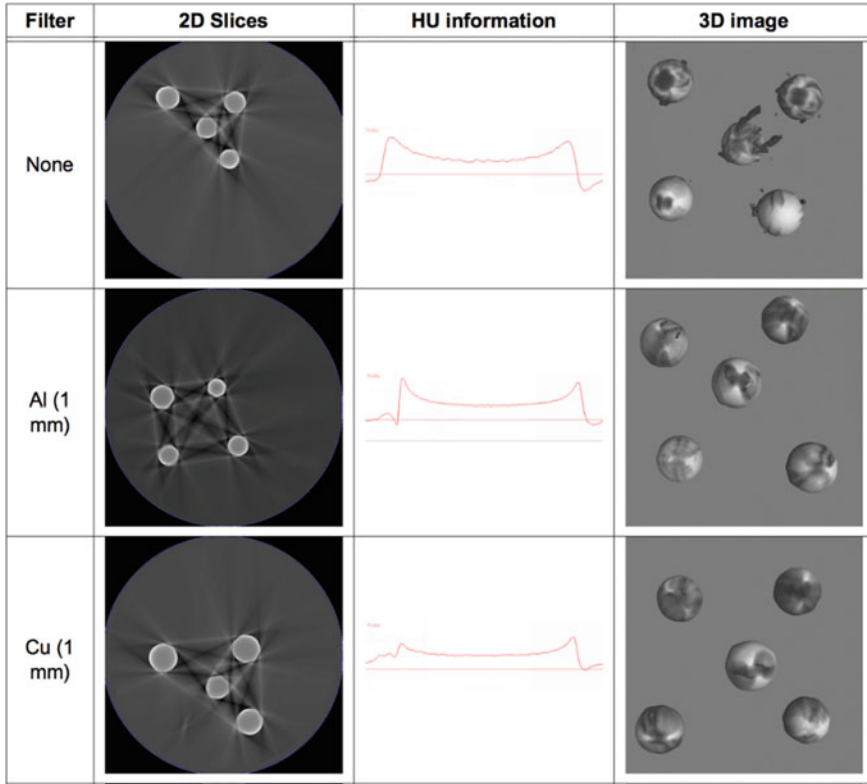| Filter	2D Slices	HU information	3D image
None			
Al (1 mm)			
Cu (1 mm)			

Fig. 3.4 CT number profile across the centre of a phantom (containing uniform shotgun pellets) showing cupping (brighter edges to the pellet) and streaking artefacts and the effect of using different filters on the profile obtained

source and the sample. These filters are typically thin (0.5–mm– thick) metal sheets of copper, tin or aluminium. An example of a cupping artefact from imaging shot–gun pellets is shown in Fig. 3.4, and the way in which filters change the shape of the artefact can also be seen. The disadvantage of using physical filters is that it reduces the signal–to–noise ratio.

Beam hardening artefacts can also be reduced by using correction algorithms in the image analysis.

Another type of artefact is a streak artefact. These usually occur when the X–ray beam is completely attenuated by high–density objects, but can also be caused by detectors with limited dynamic range, those with a limited number of discrete levels of measurement between the maximum and minimum signal that can be registered, such that peak white and peak black are readily reached and useful information from the image is lost.

Noise artefacts arise from two sources: structured noise from instrument artefacts such as electronic noise and detector inefficiency and random statistical noise from

background radiation [31]. Noise artefacts can be reduced by increasing the signal to noise ratio (SNR) i.e. by increasing the number of X–rays the sample is exposed to. Image processing methods such as averaging can also be used when using reconstruction software. One of the concerns about noise (in both medical and industrial CT) is that it can lead to false positive readings (for example, noise can appear as dots which could be mistaken for nodules in tissue samples [32] or pores or cavities in castings in industrial components [33]).

Partial Volume Artefacts

Each voxel in a CT image represents the attenuation properties of the specific material within the voxel. Partial volume effects or artefacts occur when a single voxel is filled by substances of two widely different absorptions. This gives a beam attenuation that is reflective of the average HU value of the substances. This can cause challenges in interpreting images quantitatively, particularly around boundaries. In materials and geology these effects can be used to highlight cracks or porosity and can add value; however, the image interpretation can be more challenging. Sutton et al. [34] suggest that partial volume effects are most problematic when the anatomical structure is close to the voxel size and that the way of reducing the issue is either increased magnification or else a detector with greater dimensions.

Scanner–based Sources of Error

There are a number of different errors that can arise from the μCT system itself. One of these is beam drift, where the spatial location of the X–ray focal spot can move or drift as the X–ray tube thermally expands. X–rays are typically generated by heating a filament of a material, usually tungsten that generates an electron beam that hits a target that then emits the X–rays. The temperature of the X–ray tube has to be controlled by cooling so that any errors from thermal drift are eliminated. Another issue related to the detectors, are concentric ring artefacts. These occur either from defects in the detectors themselves, poor detector calibration or non–uniform output from channel to channel in the detector array. Ring artefacts can be removed by carefully controlling the sensitivity across the whole detector to be uniform or using a numerical algorithm to correct for the issue.

Radiation Damage

Micro–computed tomography is largely considered to be non–destructive but as voxel sizes become smaller, the X–ray dose required to produce a high–quality radiograph increases. The high radiation dose can lead to radiation artefacts and damage to samples which might otherwise be considered to be macroscopically undamaged. The dose can cause damage to DNA, lead to discoloration or create chemical or structural damage for example. The radiation exposure of the object being studied increases with the voxel side dimension to the 4th power. Thus, higher spatial resolutions give increased radiation exposure. The higher energy X–rays in tube source μCTs are considered less damaging than X–rays used in nano-CT from synchrotron sources which are usually lower energy X-rays with energies in the range soft (<1 keV) or moderate (5–30 keV) [18] but when also combined with the higher X-ray flux from a synchrotron source leads to a higher dose on the sample.

Immel et al. [35] studied subfossil bones and identified that a dose of <200 Gy was the safe limit to prevent DNA damage. In order to achieve doses less than this the CT voxel sizes needed to be >1 μm. Immel et al. [35] also suggested that a metallic filter should be used between the source and the sample to filter out the lowest energy and most damaging X–rays from the whitebeam radiation. McCollough et al. [36] found that the dose for a head scanned in a medical scanner is typically of the order of 0.06 Gy which should be low enough to avoid denaturing any DNA. For a 100 kV tube source CT with a 10 μm voxel size, Meganeck et al. [37] showed that the dose is ~0.4 Gy which again should be within acceptable limits.

Selected Applications

Bones and Toolmarks

Thali et al. [38] showed that μCT could be used for investigating knife marks in bones. The shape and size of the mark could indicate the type of tool used to make the mark. 3D analysis of the marks could be used to generate a "digital virtual knife", and hence bone injuries could be correlated to the knife that made them. General class characteristics such as size, profile, shape, direction of travel and movement in the wound could also be visualised. Pounder and Sim [39] used μCT to investigate the serrations left by serrated knifes in stab wound tracts. Rutty et al. [19] demonstrated how the 3D sectioning of images through saw tracts could be used to differentiate between knife and saw marks from the shape of the bottom of false start kerfs and also showed the advantage that μCT has in reducing specular reflection (from mirror–like reflection of visible light) that is common in optical microscope images of tool marks on bone. Further work on investigating the use of μCT on marks made with different saws was performed by Norman et al. [40], who made cut marks with hand and electric saws and analysed the information that could be obtained. They found that
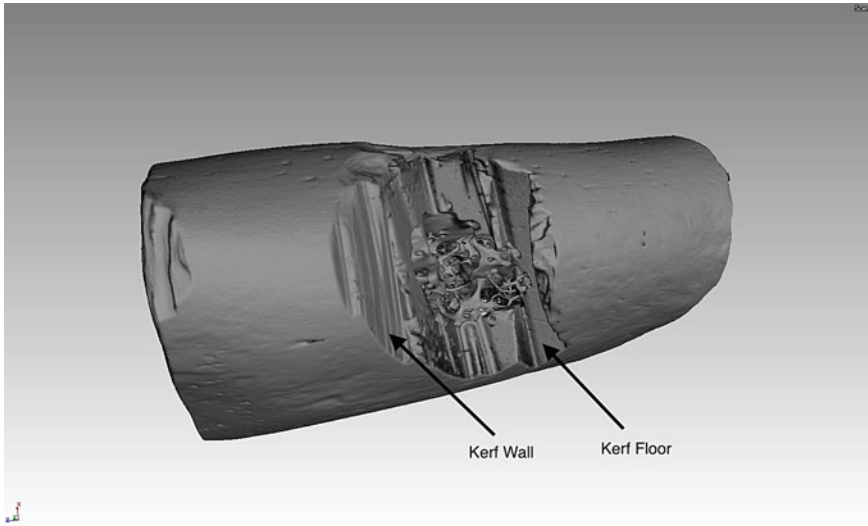
Fig. 3.5 Reconstruction of a μCT image of a partial cut through a jaw bone with an electrically powered circular saw. A number of steps can be seen in the kerf wall and the kerf (cut) floor is clearly visible. Partial cuts such as this can be used to potentially determine the thickness of the cutting blade

the width of the tool marks obtained from μCT could be consistently matched to the saw blade width and that marks made in fleshed bone were different to those made in defleshed bone. Norman et al. also produced an extended study of tool marks in bone from various different knives [41]. μCT analysis of weapon marks on bones can also be applied to archaeological cases such as analysis of the weapon marks on the remains of Richard III [42].

Figure 3.5 gives an example of the information that can be obtained from a μCT image.

The image shows a 3D reconstruction of a μCT image of a partial cut made with an electrically powered circular saw through a jaw bone. A number of steps can be seen in the kerf wall and the kerf (cut) floor is clearly visible. Partial cuts such as this can be used to potentially determine the thickness of the cutting blade. An additional advantage of using μCT in dismemberment cases is that the images are reconstructions and therefore can be shown in court in a way that pathology photographs cannot be shown. A further advantage of the 3D data is that it can be used along with 3D printing to provide replicas which again can be shown in court [43].

Larynx Fractures

Strangulation is a challenging cause of death to diagnose and a common homicide method, particularly for women who are commonly strangled by their partners. One of the challenges for the forensic pathologist is that the injuries can be subtle with no obvious bruising or compression of the neck and with a lack of features that can be attributed to asphyxia.

A number of authors have used μCT for analysing strangulation cases [44]. Baier [45] performed a comprehensive set of scans in which larynxes from a control group were imaged using μCT and compared to the current "gold standard" of histology. They examined two larynges from suspected strangulations and showed a strong correlation between the histology and the μCT images.

An example of a fractured larynx is shown in Fig. 3.6 (image courtesy of Prof Mark Williams of the University of Warwick). The fractures are labelled as A for a fracture on the posterior right greater horn and B for a fracture on the thyroid laminae. There was also a possible fracture identified at the base of the left superior horn of the thyroid cartilage.

The disadvantage of μCT for analysing injuries such as this is that the soft–tissue injuries cannot be readily visualised but it does show the benefit of using this technique for analysing fractures that cannot be seen on a conventional MDCT used for post–mortem virtopsys.

Fig. 3.6 An antero-lateral view of the volume-rendered μCT scan of a larynx A = hyoid fracture, B = fracture on left inferior margin of thyroid lamina, C = possible fracture of left superior thyroid horn

Gunshot

Analysis of gunshot residue is important for understanding the firing range in fatalities from gunshot. μCT has been used for detection of gunshot residue (GSR) in firearm wounds [46] and also for estimating firing distances from residue around gunshot wounds [47]. This work showed how μCT was able to generate a 3D reconstruction of the spatial distribution of GSR particles.

Giraudo et al. [48] performed detailed studies on the analysis of gunshot residue on wounds from a 0.32ACP pistol (Berretta Mod. 81) when the shots were made through fabrics as most shooting injuries are made when the victim is clothed. The shots were fired into sections of human calves at three different muzzle–to–target distances. All entrance wounds showed evidence of radio–opaque materials, whereas no exit wounds showed any evidence of GSR. This showed the value of μCT as a potential screening tool for differentiating between entrance and exit wounds.

μCT can also be used to evaluate the distribution of shot gun pellets into a sample. Figure 3.7 shows how the distribution of pellets from a shot gun discharged into a butchered pig's leg can be determined using μCT. The image shows the results from a test shot made using a Spanish Laurona 12–Bore Over/Under 28″ barrel shotgun with the lower barrel having a quarter choke. The ammunition was a twelve–gauge shot cartridge with plastic wadding. The figure shows that the pellets stop at differing distances into the leg, with a band of pellets towards the bottom of the figure at the point at which the pellets do not have sufficient energy to penetrate further into the
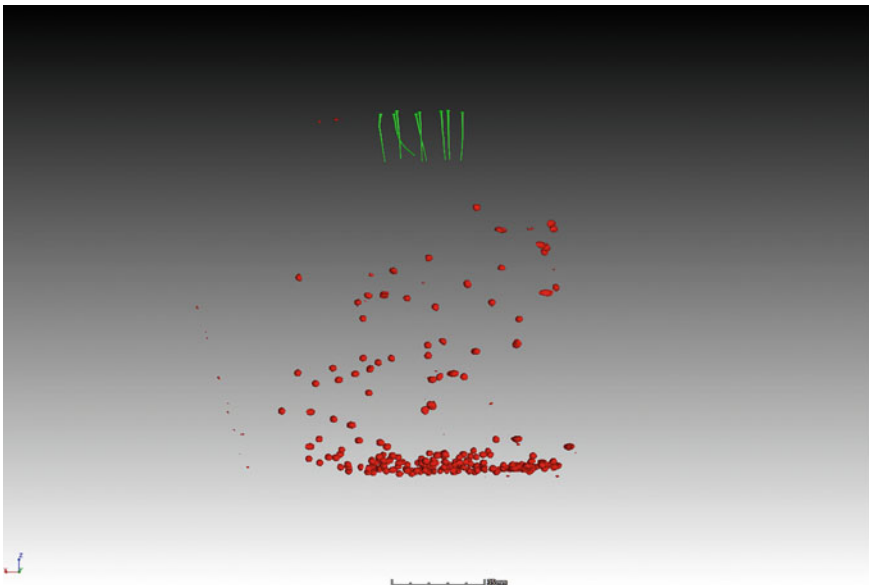

Fig. 3.7 μCT image of shotgun pellets into a pig's legs. Pellets are shown in red. The entrance wound position is marked by the green pins

flesh. The surface of the skin which was difficult to see with the μCT analysis, was marked by pins which are shown in green. The surface was not straightforward to determine as it was difficult to manipulate the image because of the large contrast range between the flesh and pellets. The pins therefore gave a convenient way of accurately determining the position of the entrance wounds.

A range of experiments were undertaken with differing firing distances into a butchered pig's leg from contact (0 m), 1 m, 2 m, 3 m, and 4 m and these could be correlated against the depth of penetration of pellets into a victim with closer–range shots penetrating to further distances. The spread (scatter) of the pellets also increased as the distance of the muzzle from the leg increased.

Entomology

Benecke [49] suggested that forensic entomology became identifiable as a discipline after the first use of insects and other arthropods as forensic indicators in Germany and France in the late by Reinhard and Hofmann; although there are case reports from China as early as the 13th Century of flies being found on deceased bodies. Bergeret, a French physician, is attributed as the first to use blow–fly pupae and larval moths [49] for determining postmortem interval (PMI) which is defined as the period between the time of death of a cadaver and when it was discovered. PMI is challenging to determine accurately as there are a large number of variables that affect the rate of decomposition of a cadaver, but forensic entomology is deemed useful in estimating the time since death with an acceptable degree of confidence to aid investigation [50]. Different insects and animals are interested in the cadaver at different stages of the cadaver decomposition [51].

Calliphora vicinia and *Calliphora vomitoria* [50] are the most common blowfly species in the UK and are the first to conquer a fresh cadaver [52].

It is often difficult to determine the age of a blowfly during the pupation stage as the fly is cocooned in a casing and the external features of the cocoon look very similar over the entire developmental stage. Figure 3.8 shows the different developmental stages of the pupae.

The traditional method for determining the pupal development stage is to use an invasive technique where the pupae is killed, stained, and dissected [52–54].

μCT is ideal for investigating the different stages of the pupal development as the internal 3D structure of the cocoon can be examined. Richards et al. [55] used μCT to scan *Calliphora vicina (Diptera: Calliphoridae)* during metamorphosis and reconstructed the internal structures of the pupae. Their work showed that μCT was a viable and a better alternative to the traditional methods. Martín–Vega et al. [56] were able to track the development of pupae, determine the critical periods in its development, and understand the role of the gas bubble during the structural development of the flies with unprecedented detail.
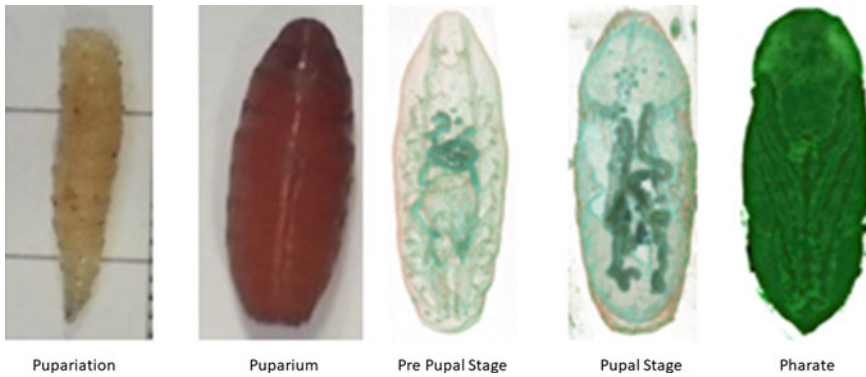
| Pupariation | Puparium | Pre Pupal Stage | Pupal Stage | Pharate |

Fig. 3.8 The different phases of the pupal development

A series of images of blow–fly larvae at different stages of development were scanned in a Nikon XT H 225 industrial micro–CT scanner controlled by Nikon Inspect–X software with the parameters below:

1. 60 kV and 70 μA
2. 700 ms exposure
3. 0.5 mm tin filter

Pupae were held in place in the scanner by inserting them into a paper drinking straw which was found to give a way of obtaining images of several pupae in a single scan with good mechanical stability of the pupae.

The images were pre-processed using the scanner software and then uploaded to VGI Studio MAX where the air phase of the sample was removed. These files were then uploaded to Image-J to remove any noise and to create sharper and better-contrasted stacks of images. The image stacks were then uploaded to Drishti where the stacks of images were compiled into a 3D model that could be rendered and processed. In Drishti the scans were put through a series of morphological operations to expose the external and internal features of the fly within the pupae. Images of the scans were then collected and arranged to show the progression in the development of the pupae. Pupae were developed at a range of temperatures and for a varying number of days.

Figure 3.9 shows the development of a pupae at 2, 7 and 8 days. The μCT scans gives an understanding of the internal structure within the epidermis. This was especially convenient during the first few days after the puparium formation where the early tracheal tube structure (A), coiled tubular cluster (B) and gas bubble (C) is easily seen.
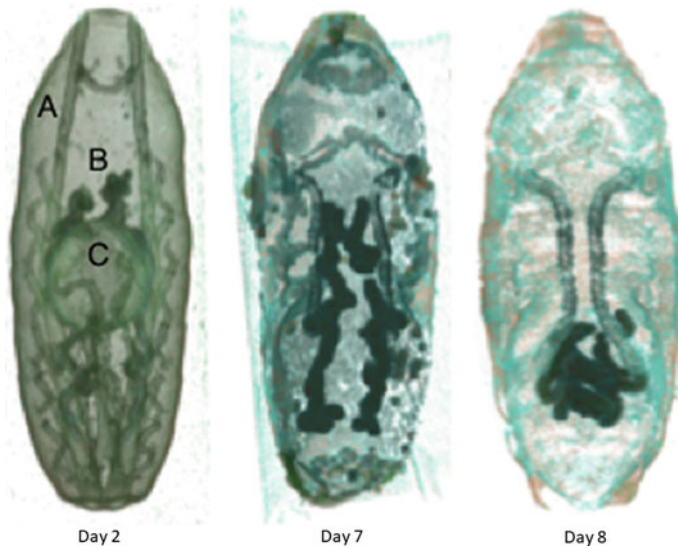
Fig. 3.9 Pupae development from μCT imaging illustrating the change in the tracheal tube and coiled tubed cluster as the pupae mature. A is the early tracheal tube, B the coiled tubular cluster and C the gas bubble

The point where the change from pre–pupal stage to pupal stage was also definite, and allowed the apolysis to be observed and the change in the tracheal tube structure to be visualised. Additionally, the progression of the coiled tubular cluster as well as its change in position overtime can be seen in the images.

However, in comparison to features that can be identified by traditional methods there are a number of structures that are not visible on the μCT images:– for example, the central nervous system, the peripheral nervous system, and the muscles along the body are not readily visible [57].

The full power of μCT as a visualisation tool for the internal structures can be seen in images in Fig. 3.10.

One of the advantages of μCT scanning is that in many instances, for example, in the imaging of blow–fly internal structures, the evolution of structure whilst an organism is growing can be tracked with multiple scanning sessions over a period of time.

A previous study on the radiation of Mexican fruit–fly suggests that the third –instar larvae and prepupal stage pupae have low sensitivity to irradiation, and the pupae are thought to be able to recover after each dose [58]. However, scans by us found that only small numbers of irradiated pupae emerged compared to their non–radiated counterpart, when each sample was only scanned once. Our scans were conducted to minimise exposure to radiation and therefore the image quality is less than if longer scans were used and therefore there is a compromise between development and quality of information obtained during μCT scanning.
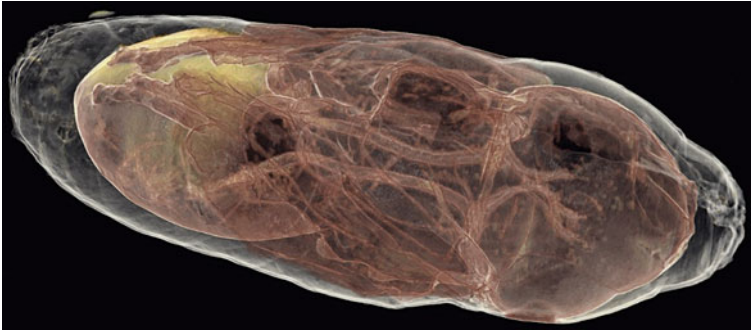
Fig. 3.10 Image of a blow fly pupae from X–ray µCT images using Drishti post processing to reveal and colour the structures that have developed

The scans in Figs. 3.8 and 3.9 were obtained without the use of staining as would be required in traditional studies using reflected light microscopy. Stains are not always required for µCT investigations. However, some researchers, such as Metscher, Kang et al. and Swart et al. [59–61] have used staining to provide additional contrast which improves the discrimination of the internal structure for studies of blow–flies and barnacles. Not all contrast stains are inert, and some may damage the specimen. Pauwels et al. [62] noted that acids such as phosphotungstic acid (PTA), dodeca molybdophosphoric acid (PMA) and FeCl$_3$ solution when used in high concentrations can dissolve calcified tissues such as bones and thereby destroy the specimen being examined.

The choice of staining therefore depends on what the aim of the investigation is. For fundamental science or entomology staining may be desirable but there will be instances where a forensic sample must remain unchanged unless experts for both prosecution and the defence agree that staining is an acceptable method from both parties' perspective.

Summary

Micro X–ray Computed Tomography has developed over the last 30 years as digital X–ray detectors have allowed the capture of multiple radiographs that can be reconstructed to give a 3D representation of the sample.

During this period, the time required to obtain the scans has reduced, and the computing power of the systems to generate the 3D images has evolved at pace. The power of the technique means that it has found multiple practical applications in the areas of forensic science and engineering. Continuous improvements in the image resolution and image contrast are likely to for the foreseeable future.

One particular advantage of the technique for forensic applications is that the images are traceable and easily shared, and the data can readily be stored. By comparison to multi–detector computed tomography scans that are commonly used for autopsy, μCT offers access to higher magnifications and higher resolutions, which means that it offers additional functionality and possibilities for forensic applications.

As access to scanners improves and the software and interpretation of images becomes more accessible, the diversity of applications in forensic science continues to grow. μCT therefore adds powerful additional insights for the forensic practitioner to interpret and understand forensic case work.

References

1. Mould RF. The early history of X-ray diagnosis with emphasis on the contributions of physics 1895–1915. Phys Med Biol. 1995;40(11):1741–87. https://doi.org/10.1088/0031-9155/40/11/001.
2. DenOtter TD, Schubert J. Hounsfield unit. Treasure Island (FL): StatPearls Publishing; 2022.
3. Glide-Hurst C, Chen D, Zhong H, Chetty IJ. Changes realized from extended bit-depth and metal artifact reduction in CT. Med Phys. 2013;40(6):61711. https://doi.org/10.1118/1.4805102.
4. Eckert WG, Garland N. The history of the forensic application in radiology. Amer J Forensic Med Pathol. 1984;5(1).
5. Blakeley C, Hogg P. Manchester medical society (imaging section) presidential address 2008. Radiography; 2009. https://doi.org/10.1016/j.radi.2009.10.001.
6. Di Chiro G, Brooks RA. The 1979 nobel prize in physiology or medicine. J Comput Assist Tomogr. 1980;4(2):241–5. https://doi.org/10.1097/00004728-198004000-00023.
7. Tempany CMC, McNeil BJ. Advances in biomedical imaging. J Am Med Assoc. 2001;285(5):562–7. https://doi.org/10.1001/jama.285.5.562.
8. Kalender WA. X-ray computed tomography. Phys Med Biol. 2006;51(13):R29–43. https://doi.org/10.1088/0031-9155/51/13/r03.
9. Saunders SL, Morgan B, Raj V, Rutty GN. Post-mortem computed tomography angiography: past, present and future. Forensic Sci Med Pathol. 2011;7(3):271–7. https://doi.org/10.1007/s12024-010-9208-3.
10. Leth P. The use of CT scanning in forensic autopsy. Forensic Sci Med Pathol. 2007;3:65–9. https://doi.org/10.1385/FSMP:3:1:65.
11. Flohr TG, Schaller S, Stierstorfer K, Bruder H, Ohnesorge BM, Schoepf UJ. Multi–detector row CT systems and image-reconstruction techniques. Radiology. 2005;235(3):756–73. https://doi.org/10.1148/radiol.2353040037.
12. Rutty GN, Morgan B. Virtual autopsy. Forensic Sci Med Pathol. 2013;9(3):433–4. https://doi.org/10.1007/s12024-013-9450-6.

13. Brüllmann D, Schulze RKW. Spatial resolution in CBCT machines for dental/maxillofacial applications-what do we know today? Dentomaxillofac Radiol. 2015;44(1):20140204. https://doi.org/10.1259/dmfr.20140204.

14. Pauwels R, Araki K, Siewerdsen JH, Thongvigitmanee SS. Technical aspects of dental CBCT: state of the art. Dentomaxillofac Radiol. 2015;44(1):20140224. https://doi.org/10.1259/dmfr.20140224.

15. Dawood A, Patel S, Brown J. Cone beam CT in dental practice. Br Dent J. 2009;207(1):23–8. https://doi.org/10.1038/sj.bdj.2009.560.

16. O'Connell A, et al. Cone-beam CT for breast imaging: radiation dose, breast coverage, and image quality. Am J Roentgenol. 2010;195(2):496–509. https://doi.org/10.2214/AJR.08.1017.

17. Ritman EL. Current status of developments and applications of Micro-CT. Annu Rev Biomed Eng. 2011;13(1):531–52. https://doi.org/10.1146/annurev-bioeng-071910-124717.

18. Withers PJ, et al. X-ray computed tomography. Nature Rev Methods Primers. 2021;1(1):18. https://doi.org/10.1038/s43586-021-00015-4.

19. Rutty GN, Brough A, Biggs MJP, Robinson C, Lawes SDA, Hainsworth SV. The role of micro-computed tomography in forensic investigations. Forensic Sci Int; 2013. https://doi.org/10.1016/j.forsciint.2012.10.030.

20. Sun W, Brown S, Leach R. An overview of industrial X-ray computed tomography; 2011.

21. Carmignato S, Dewulf W, Leach R. Industrial X-ray computed tomography. Springer International Publishing; 2018.

22. du Plessis A, le Roux SG, Guelpa A. Comparison of medical and industrial X-ray computed tomography for non-destructive testing. Case Stud Nondestruct Testing Eval. 2016;6:17–25. https://doi.org/10.1016/j.csndt.2016.07.001.

23. Christensen A, Smith M, Gleiber D, Cunningham D, Wescott D. The Use of X-ray computed tomography technologies in forensic anthropology. Forensic Anthropol. 2018;1:124–40. https://doi.org/10.5744/fa.2018.0013.

24. Bolliger SA, Oesterhelweg L, Spendlove D, Ross S, Thali MJ. Is differentiation of frequently encountered foreign bodies in corpses possible by hounsfield density measurement? J Forensic Sci. 2009;54(5):1119–22. https://doi.org/10.1111/j.1556-4029.2009.01100.x.

25. McCullough EC, et al. Performance evaluation and quality assurance of computed tomography scanners, with illustrations from the EMI, ACTA, and delta scanners. Radiology. 1976;120(1):173–88. https://doi.org/10.1148/120.1.173.

26. Rueckel J, Stockmar M, Pfeiffer F, Herzen J. Spatial resolution characterization of a X-ray microCT system. Appl Radiat Isot. 2014;94:230–4. https://doi.org/10.1016/j.apradiso.2014.08.014.

27. Schladitz K. Quantitative micro-CT. J Microsc. 2011;243(2):111–7. https://doi.org/10.1111/j.1365-2818.2011.03513.x.

28. Feldkamp LA, Davis LC, Kress JW. Practical cone-beam algorithm. J Opt Soc Am A. 1984;1(6):612–9. https://doi.org/10.1364/JOSAA.1.000612.

29. Limaye A. Drishti: a volume exploration and presentation tool. In: Proceedings SPIE, 2012, vol. 8506, pp. 85060X–8506–9. https://doi.org/10.1117/12.935640.

30. Schneider CA, Rasband WS, Eliceiri KW. NIH Image to ImageJ: 25 years of image analysis. Nat Methods. 2012;9(7):671–5. https://doi.org/10.1038/nmeth.2089.

31. Cherry SR, Sorenson JA, Phelps MEBT. Physics in nuclear medicine, 4th Editio. Philadelphia: Elsevier, 2012. https://doi.org/10.1016/B978-1-4160-5198-5.00033-2.

32. Kamiyama H, et al. Unusual false-positive mesenteric lymph nodes detected by PET/CT in a metastatic survey of lung cancer. Case Rep Gastroenterol. 2016;10(2):275–82. https://doi.org/10.1159/000446579.

33. Fuchs P, Kröger T, Garbe CS. Defect detection in CT scans of cast aluminum parts: a machine vision perspective. Neurocomputing. 2021;453:85–96. https://doi.org/10.1016/j.neucom.2021.04.094.

34. Sutton M, Rahman I, Garwood R. Techniques for virtual. Palaeontology. 2014. https://doi.org/10.1002/9781118591192.

35. Immel A, et al. Effect of X-ray irradiation on ancient DNA in sub-fossil bones—Guidelines for safe X-ray imaging. Sci Rep. 2016;6:32969. https://doi.org/10.1038/srep32969.
36. McCollough CH, Bushberg JT, Fletcher JG, Eckel LJ. Answers to common questions about the use and safety of CT scans. Mayo Clin Proc. 2015;90(10):1380–92. https://doi.org/10.1016/j.mayocp.2015.07.011.
37. Meganck JA, Liu B. Dosimetry in micro-computed tomography: a review of the measurement methods, impacts, and characterization of the quantum GX imaging system. Mol Imag Biol. 2017;19(4):499–511. https://doi.org/10.1007/s11307-016-1026-x.
38. Thali M, et al. Forensic microradiology: micro-computed tomography (Micro-CT) and analysis of patterned injuries inside of bone. J Forensic Sci. 2003;48:1336–42. https://doi.org/10.1520/JFS2002220.
39. Pounder DJ, Sim LJ. Virtual casting of stab wounds in cartilage using micro-computed tomography. Amer J Forensic Med Pathol. 2011;32(2). [Online]. Available: https://journals.lww.com/amjforensicmedicine/Fulltext/2011/06000/Virtual_Casting_of_Stab_Wounds_in_Cartilage_Using.1.aspx.
40. Norman DG, Baier W, Watson DG, Burnett B, Painter M, Williams MA. Micro-CT for saw mark analysis on human bone. Forensic Sci Int. 2018;293:91–100. https://doi.org/10.1016/j.forsciint.2018.10.027.
41. Norman DG, Watson DG, Burnett B, Fenne PM, Williams MA. The cutting edge—Micro-CT for quantitative toolmark analysis of sharp force trauma to bone. Forensic Sci Int. 2018;283:156–72. https://doi.org/10.1016/j.forsciint.2017.12.039.
42. Appleby J, et al. Perimortem trauma in King Richard III: a skeletal analysis. The Lancet. 2015;385(9964):253–9. https://doi.org/10.1016/S0140-6736(14)60804-7.
43. Biggs M. 3D printing applied to forensic investigations. In: Essentials of autopsy practice 2019, pp. 19–49. https://doi.org/10.1007/978-3-030-24330-2_2.
44. Fais P, et al. Micro computed tomography features of laryngeal fractures in a case of fatal manual strangulation. Leg Med. 2016;18:85–9. https://doi.org/10.1016/j.legalmed.2016.01.001.
45. Baier W, Mangham C, Warnett JM, Payne M, Painter M, Williams MA. Using histology to evaluate micro-CT findings of trauma in three post-mortem samples—First steps towards method validation. Forensic Sci Int. 2019;297:27–34. https://doi.org/10.1016/j.forsciint.2019.01.027.
46. Cecchetto G, et al. MicroCT detection of gunshot residue in fresh and decomposed firearm wounds. Int J Legal Med. 2012;126(3):377–83. https://doi.org/10.1007/s00414-011-0648-4.
47. Cecchetto G, et al. Estimation of the firing distance through micro-CT analysis of gunshot wounds. Int J Legal Med. 2011;125(2):245–51. https://doi.org/10.1007/s00414-010-0533-6.
48. Giraudo C, et al. Micro-CT features of intermediate gunshot wounds covered by textiles. Int J Legal Med. 2016;130(5):1257–64. https://doi.org/10.1007/s00414-016-1403-7.
49. Benecke M. A brief history of forensic entomology. Forensic Sci Int. 2001;120(1):2–14. https://doi.org/10.1016/S0379-0738(01)00409-1.
50. Gennard DE. Forensic entomology: an introduction. Chichester, England: Wiley; 2012.
51. Anderson GS. The use of insects in death investigations: an analysis of cases in British Columbia over a five year period. Canadian Soc Forensic Sci J. 1995;28(4):277–92. https://doi.org/10.1080/00085030.1995.10757488.
52. Greenberg B. Flies as forensic indicators. J Med Entomol. 1991;28(5):565–77. https://doi.org/10.1093/jmedent/28.5.565.
53. Sukontason KL, et al. Morphological observation of puparia of Chrysomya nigripes (Diptera: Calliphoridae) from human corpse. Forensic Sci Int. 2006;161(1):15–9. https://doi.org/10.1016/j.forsciint.2005.10.013.
54. Sert O, Ergil C. An examination of the intrapuparial development of Chrysomya albiceps (Wiedemann, 1819) (Calliphoridae: Diptera) at three different temperatures. Forensic Sci Med Pathol. 2021;17(4):585–95. https://doi.org/10.1007/s12024-021-00411-y.
55. Richards CS, Simonsen TJ, Abel RL, Hall MJR, Schwyn DA, Wicklein M. Virtual forensic entomology: improving estimates of minimum post-mortem interval with 3D micro-computed tomography. Forensic Sci Int. 2012;220(1):251–64. https://doi.org/10.1016/j.forsciint.2012.03.012.

56. Martín-Vega D, Simonsen TJ, Hall MJR. Looking into the puparium: Micro-CT visualization of the internal morphological changes during metamorphosis of the blow fly, Calliphora vicina, with the first quantitative analysis of organ development in cyclorrhaphous dipterans. J Morphol. 2017;278(5):629–51. https://doi.org/10.1002/jmor.20660.
57. Chyb S, Gompel N. Atlas of drosophila morphology : wild-type and classical mutants. Amsterdam: Academic Press; 2013.
58. Thomas DB, Hallman GJ. Developmental Arrest in Mexican Fruit Fly (Diptera: Tephritidae) Irradiated in Grapefruit. Ann Entomol Soc Am. 2011;104(6):1367–72. https://doi.org/10.1603/AN11035.
59. Metscher BD. MicroCT for comparative morphology: simple staining methods allow high-contrast 3D imaging of diverse non-mineralized animal tissues. BMC Physiol. 2009;9:11. https://doi.org/10.1186/1472-6793-9-11.
60. Kang V, Johnston R, van de Kamp T, Faragó T, Federle W. Morphology of powerful suction organs from blepharicerid larvae living in raging torrents. BMC Zoology. 2019;4(1):10. https://doi.org/10.1186/s40850-019-0049-6.
61. Swart P, Wicklein M, Sykes D, Ahmed F, Krapp HG. A quantitative comparison of micro-CT preparations in Dipteran flies. Sci Rep. 2016;6(1):39380. https://doi.org/10.1038/srep39380.
62. Pauwels E, van Loo D, Cornillie P, Brabant L, van Hoorebeke L. An exploratory study of contrast agents for soft tissue visualization by means of high resolution X-ray computed tomography imaging. J Microsc. 2013;250(1):21–31. https://doi.org/10.1111/jmi.12013.